IRAM-531

A HIGH-RESOLUTION STUDY OF EPISODIC MASS LOSS FROM THE CARBON STAR TT CYGNI

H. Olofsson, P. Bergman, R. Lucas,
K. Eriksson, B. Gustafsson, J.H. Bieging

IRAM N° 531

To be published in
Astronomy & Astrophysics

1999

A&A manuscript no.
(will be inserted by hand later)

Your thesaurus codes are:
06(08.03.1; 08.03.4; 08.09.2 TT Cyg; 08.13.2; 13.19.5)

ASTRONOMY AND ASTROPHYSICS
November 1, 1999

A high-resolution study of episodic mass loss from the carbon star TT Cygni

H. Olofsson[1], P. Bergman[2], R. Lucas[3], K. Eriksson[4], B. Gustafsson[4], and J.H. Bieging[5]

[1] Stockholm Observatory, SE-133 36 Saltsjöbaden, Sweden
[2] Onsala Space Observatory, SE-439 92 Onsala, Sweden
[3] IRAM, 300, rue de la Piscine, F-38406 Grenoble-Cedex, France
[4] Uppsala Astronomical Observatory, Box 515, SE-751 20 Uppsala, Sweden
[5] Steward Observatory, Univ. of Arizona, Tucson, AZ 85721, USA

Not KW

Received date; accepted date

Abstract. CO radio line observations with the IRAM Plateau de Bure interferometer show that the carbon star TT Cyg is surrounded by a large (radius $\sim$35″ or 2.7×10^{17} cm), geometrically thin (average width $\sim$2″.5 or 1.9×10^{16} cm) shell of gas, which has a remarkable overall spherical symmetry (e.g., its radius varies by less than $\pm$3%). It expands with a velocity of $\sim$12.6 km s^{-1}. The emitting gas is very evenly distributed in the shell when averaged over a solid angle of about 0.2 steradians. We estimate a molecular hydrogen density of $\sim$250 cm^{-3}, a gas kinetic temperature of $\sim$100 K, and a mass of $\sim$0.007 M$_\odot$ for the shell if the medium is homogeneous. There is no evidence for matter immediately inside or outside the shell, nor is there any evidence for structure in the radial direction of the shell brightness distribution (it is essentialy perfectly fitted with Gaussians). The shell centre is displaced $\sim$1″.7 (position angle $\sim$–20°) with respect to the star. We favour an interpretation of this displacement in terms of TT Cyg being a member of a binary system. We put forward several arguments for a shell medium that consists almost entirely of a large number of small ($\lesssim$1″) clumps (in which case the density required to fit the observational data is much higher, $\sim10^4$ cm^{-3}, and the kinetic temperature is considerably lower, $\lesssim$20 K). TT Cyg is presently losing mass at a modest rate, $\sim3\times10^{-8}$ M$_\odot$ yr^{-1}, and with a low expansion velocity, $\sim$3.8 km s^{-1}. This is inferred from CO line emission from a region centred on the present position of the star. The systemic velocity is estimated, from both the centre and the shell emission, to be –27.3$\pm$0.1 km s^{-1} in the LSR system. All quantitative results are obtained assuming the Hipparcos distance of 510 pc.

These data strongly support that TT Cyg has recently ($\sim7\times10^3$ yr ago) gone through a period of drastically varying mass loss properties. We discuss briefly two scenarios: a short period (a few hundred years) of very intense mass loss (a rate in excess of 10^{-5} M$_\odot$ yr^{-1}), and a related scenario with a more modest mass ejection and where most of the shell gas is swept-up from a previous, slower stellar wind. It is presently not possible to favour any of these two scenarios, but we suggest that in either case it is a coordinated mass ejection that caused the shell formation. The He-shell flash phenomenon in AGB-stars can provide this coordination, and it also fits the time scales involved.

Key words: Stars: carbon – circumstellar matter – Stars: individual: TT Cyg – Stars: mass-loss – Radio lines: stars

1. Introduction

Mass loss is a fundamental process during stellar evolution on the asymptotic giant branch (AGB). It limits the lifetime and the maximum luminosity reached on the AGB and puts a high lower mass limit for supernova precursors (Blöcker 1995), it affects the elemental and isotopic abundances at the stellar surface (Forestini & Charbonnel 1997) and the stellar contribution to nucleosynthesis, and it provides one of the most important replenishment processes for the interstellar medium. Even though its existence is well established, the details and the mechanism behind it remain uncertain (Olofsson 1996). It appears that the average mass loss rate increases during the AGB evolution, but there is probably also a dependence on main sequence mass, so that the more massive stars reach higher mass loss rates (Habing 1996). On shorter time scales (a few years up to $\sim10^4$ yr) there is ample evidence for variations. For instance, the marked 60μm-excesses of a number of carbon stars were interpreted as arising from detached dust shells by Willems & de Jong (1988), and for a sample of M stars by Zijlstra et al. (1992). Possibly the best examples of episodic mass loss are the detached CO and dust shells that have been detected towards seven AGB-stars, all carbon stars (Olofsson et al. 1990, 1996; Lindqvist et al. 1996, 1999; Waters et al. 1994; Izumiura et al. 1996, 1997). A similar dust shell may have been detected towards one M star (Hashimoto et al. 1998). The most spectacular result is probably the large (radius$\sim$35″) and remarkably thin CO shell found around the carbon star TT Cyg (Olofsson et al. 1998; width/radius $\lesssim$ 0.04 in the region covered by their

Send offprint requests to: H. Olofsson,
Internet: hans@astro.su.se

maps). The CO radio line emission appears to probe the mass loss history for $\sim 10^4$ yr, after which the CO molecules become rapidly photodissociated. The dust emission is maintained for a longer time, but the interpretation of these data are hampered by the poor spatial resolution.

The central stars of the 'detached shell'-systems are irregular or semiregular variables, which presently have low mass loss rate winds ($\sim 10^{-8}$–10^{-7} $M_\odot$ yr^{-1}) that expand at low velocities ($\sim$5 km s^{-1}, as opposed to the shells which expand at $\sim$15–25 km s^{-1}). The estimates of the shell masses are uncertain, but, in general the result is about 0.01 $M_\odot$ (Groenewegen & de Jong 1994; Olofsson et al. 1996; Izumiura et al. 1997). The corresponding mass loss rates depend on whether or not swept-up material plays a rôle and the time scale of ejection, which may be as low as a few hundred years as judged from the TT Cyg results (Olofsson et al. 1998). In any case, these stars have certainly gone through relatively drastic changes in their mass loss behaviour. If the process responsible for these changes can be identified, some light may also be shed on the mechanism behind the mass loss itself. So far, a connection with a He-shell flash seems the most probable explanation (Olofsson et al. 1990; Izumiura et al. 1997; Schröder et al. 1998, 1999; Steffen & Schönberner 1999). If so, these shells may be one of very few ways to investigate this astrophysically very important process.

The presence of a detached CO shell around TT Cyg was first suggested by Olofsson et al. (1990), and Olofsson et al. (1996) provided direct evidence for such a shell of diameter $\sim$70″. A high spatial resolution investigation of the CO shell around TT Cyg, using the IRAM interferometer on Plateau de Bure, was started by Olofsson et al. (1998). Here, we present interferometer observations that now cover the entire shell. At the end we discuss the constraints that these put on the possible shell formation scenarios. TT Cyg is a short-period ($\sim 120^d$) semi-regularly variable (SRb) carbon star. Its Hipparcos position is α(2000) = $19^h40^m57^s.02$, δ(2000) = 32°37′05″.7, and its galactic latitude is 4.9° with the galactic plane to the southeast along the position angle $\sim$35°. The Hipparcos distance is 510 pc, but the parallax is uncertain, 1.96±0.8 mas.

2. Observations

The CO(J=1→0 at 115 GHz, and J=2→1 at 230 GHz) observations of TT Cyg were made between November-96 and February-98 using the IRAM Plateau de Bure interferometer, France (Guilloteau et al. 1992). Five telescopes were used in four different configurations (B1, B2, C2, and D), and we observed nine primary fields in order to cover an area of about 1′.5×1′.5. The field centres were chosen in order to cover all emission in the J=1→0 line within a minimum time. The positions of the fields can be seen in the J=2→1 image in Fig. 2. The data were reduced using the GILDAS software package. The maps produced in each field were combined and deconvolved simultaneously using a generalization of the CLEAN algorithm to mosaics (Gueth et al. 1995). Natural weighting has been used for all data. The resulting images are corrected for primary beam attenuation. The synthesized beams are 2″.2×1″.8 (PA=26°) and 1″.1×0″.9 (PA=33°) for the CO(J=1→0) and CO(J=2→1) data, respectively. The velocity scale is given with respect to the Local Standard of Rest (LSR).

The entire shell is covered in the J=1→0 line, and the S/N-ratio is high as can be seen in Fig. 1, where all the data are shown at 1 km s^{-1} resolution. In the J=2→1 line the primary beam is half as wide, and only parts of the shell have been covered (we estimate that about 80% of the emitting area is covered at the systemic velocity). Thus, the mosaicing is difficult, and the final J=2→1 maps should be interpreted with caution. In Fig. 2 we show for comparison the J=1→0 and J=2→1 emissions integrated over the velocity range –27.5±2 km s^{-1}, i.e., a 4 km s^{-1} range centred close to the systemic velocity (see below). It is apparent that the S/N-ratio is much poorer in the J=2→1 line. The data clearly show the geometrical thinness of the shell, as well as the emission from a CO envelope around the star, which, in a relative sense, is more prominent in the J=2→1 data. Also shown in Fig. 2 are the total velocity-integrated J=1→0 emission, and the 1 km s^{-1} interval map centred at –38 km s^{-1}. At this velocity the line-of-sight is almost in the radial direction through the shell, and the details of the brightness distribution become more apparent. Most of the discussion in this paper will be based on the J=1→0 data.

3. Emission from the present mass loss gas

The central emission, present in both lines, presumably arises from the envelope formed during the present mass loss epoch. We have determined the peak positions by fitting two-dimensional Gaussians to the data in the –27.5±2 km s^{-1} range. The result is α(2000) = $19^h40^m57^s.00$, δ(2000) = 32°37′05″.6 and α(2000) = $19^h40^m57^s.00$, δ(2000) = 32°37′05″.9 for the J=1→0 and J=2→1 data, respectively. These positions agree, within the uncertainty of $\sim$0″.5, well with each other and with the Hipparcos position of TT Cyg.

The central J=1→0 and 2→1 brightness distributions are well fitted by circular Gaussians with deconvolved radii at half maxima of 1″.1 (corresponding to 8×10^{15} cm at the adopted distance) and 0″.8 (6×10^{15} cm) and peak brightnesses of 0.085 and 0.36 Jy beam^{-1}, respectively. That is, the emission is at least partly resolved, and the smaller size in the J=2→1 line is consistent with the higher energy requirements for exciting this line. The source fluxes, i.e., the source brightnesses integrated over the source, in the –27.5±2 km s^{-1} interval are 0.8 and 5.2 Jy km s^{-1} in the J=1→0 and J=2→1 lines, respectively. This suggests, at least partly, optically thin emission, or, as expected, that the J=2→1 line emission comes from a warmer region than the J=1→0 line. The centre position spectra are shown in Fig. 3. The J=1→0 spectrum suggests partly resolved optically thin emission, but the J=2→1 spectrum indicates a higher optical depth. The systemic and gas expansion velocities are estimated to be –27.3 km s^{-1} and 3.8 km s^{-1}, respectively. The source fluxes correspond to J=1→0 and J=2→1 line intensities of 0.03 and 0.12 K, respectively, in the

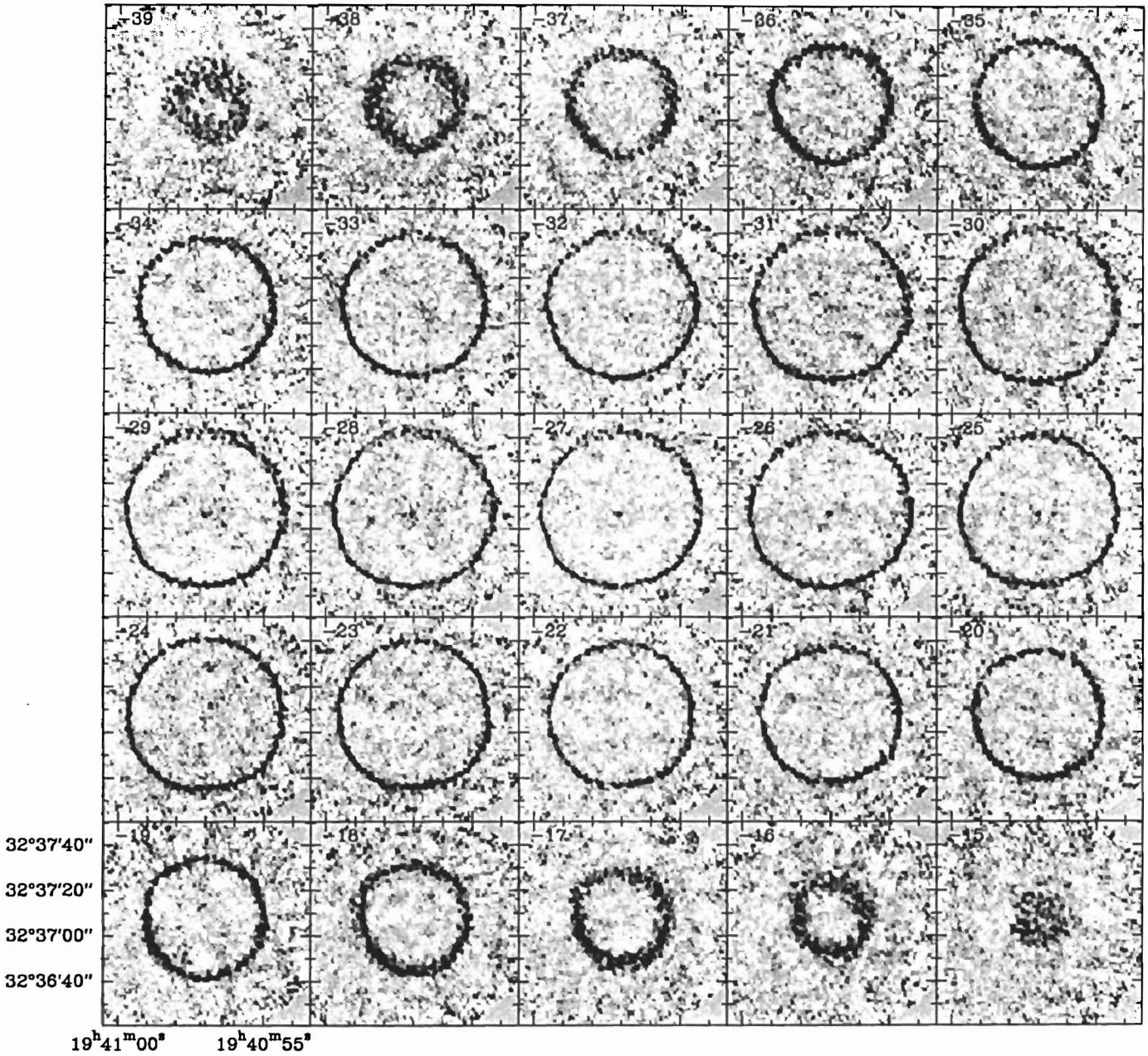

Fig. 1. CO(J=1→0) brightness maps in 1 km s^{-1} intervals (the LSR centre velocity is shown in the upper left corner of each panel) obtained towards TT Cyg. The synthesized beam is 2.″2×1.″8 (PA=26°). The systemic velocity is estimated to be –27.3 km s^{-1}

IRAM 30 m telescope (in the T_A^*-scale and assuming Gaussian sources with the estimated sizes). This is consistent with the observed intensities, ~0.05: and ~0.1 K in the J=1→0 and J=2→1 lines, respectively (Olofsson et al. 1993).

We have estimated the present mass loss of TT Cyg using these data, and a radiative transfer model that determines the excitation of the CO molecules, in a circumstellar envelope that expands with constant velocity, using the Monte Carlo method. The energy balance equation for the circumstellar gas is solved self-consistently taking into account the CO line cooling (see Schöier, PhD thesis in preparation, for details). Adopting the (uncertain) Hipparcos distance of 510 pc, a luminosity of 2300 $L_\odot$ obtained from this distance and a derived apparent bolometric magnitude, and a gas expansion velocity of 4 km s^{-1}, and assuming a stellar temperature of 2700 K, and a CO number abundance with respect to H_2, f_{CO}, of 10^{-3}, we estimate a mass loss loss rate of $\sim 3\times10^{-8}$ $M_\odot$ yr^{-1}. The J=1→0 emission is optically thin, but the J=2→1 is, at least partly, optically thick. An outer radius of the CO envelope of 3×10^{16} cm was used in order to fit the observed radial brightness distributions. This is half of that obtained from the CO photodissociation model of Mamon et al. (1988) for the derived mass loss rate, but it must be regarded as within the uncertainties of this model when applied to low mass loss rate objects.

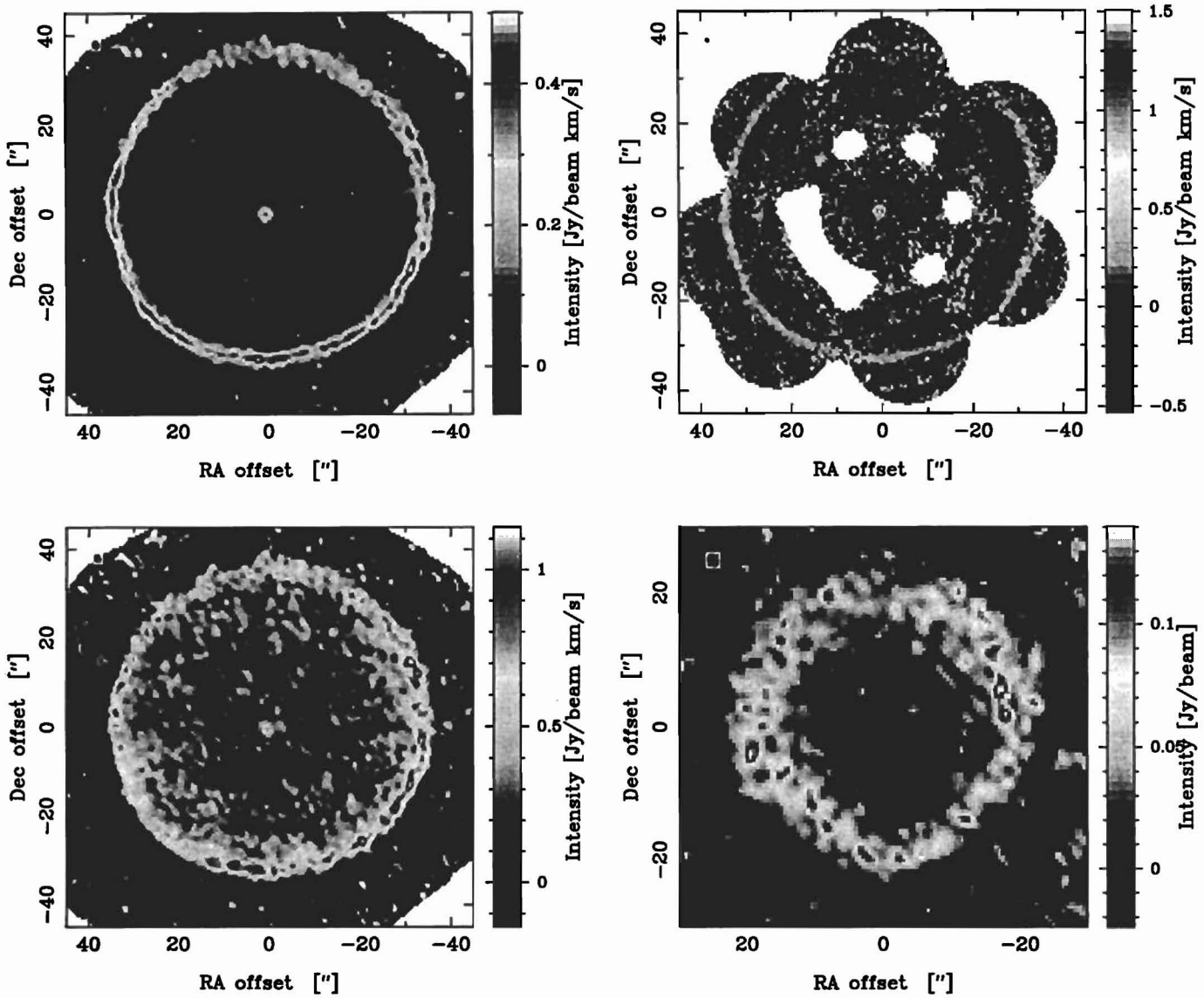

Fig. 2. CO(J=1→0 and J=2→1) brightness maps in a 4 km s^{-1} interval centred at –27.5 km s^{-1}, i.e., close to the systemic velocity (upper left and right, respectively). CO(J=1→0) velocity-integrated brightness map (lower left). CO(J=1→0) brightness map in a 1 km s^{-1} interval centred at –38 km s^{-1} (lower right). The synthesized beams are shown in the upper left corner of each panel

Thus, the present mass loss of TT Cyg lies at the very low end of the mass loss rate distribution obtained by Olofsson et al. (1993) for a sample of (~100) optically bright carbon stars. The same applies to the gas expansion velocity, which is only about one third of the median gas expansion velocity of this sample.

4. The shell emission

In this section we present the observational results for the shell emission. The analysis follows to a large extent that used in Olofsson et al. (1996, 1998). We also estimate the mass and the physical properties of the shell gas, as well as discuss the density distribution within the shell.

4.1. Comparison with single-dish fluxes

We will here estimate whether some of the total CO emission is missing in the interferometer data [see e.g. Adler et al. (1992) for a discussion of this]. We have computed the CO fluxes, integrated over the brightness distributions in four velocity ranges [the full velocity range (–40 km s^{-1}/–14.5 km s^{-1}), a velocity range centred on the systemic velocity (-29.5/–25.5), and a blue- (–40.5/–37.5) and a redshifted (–17.5/–14.5) velocity interval], using our interferometer data and the single-dish data obtained by Olofsson et al. (1996) with the IRAM 30 m telescope. The results are summarized in Table 1. For the J=1→0 line the total interferometer flux amounts to ~85% of the total single dish flux, i.e., within the calibration uncertainties it is possible that the fluxes agree, and hence very little extended

Table 1. Comparison between shell fluxes [integrated over the shell brightness distributions in four velocity ranges: the full velocity range (–40 km s^{-1}/–14.5 km s^{-1}), a range centred on the systemic velocity (-29.5/–25.5), and a blue- (–40.5/–37.5) and a redshifted (–17.5/–14.5) velocity interval] obtained from single-dish and interferometry data

	Line	S(–40.5/–14.5) [Jy km s^{-1}]	S(–40.5/–37.5) [Jy km s^{-1}]	S(–29.5/–25.5) [Jy km s^{-1}]	S(–17.5/–14.5) [Jy km s^{-1}]
IRAM interf.	$1 \rightarrow 0$	265	19	47	28
IRAM 30m	$1 \rightarrow 0$	308	36	51	40
IRAM interf.	$2 \rightarrow 1$			76	
IRAM 30m	$2 \rightarrow 1$			176	

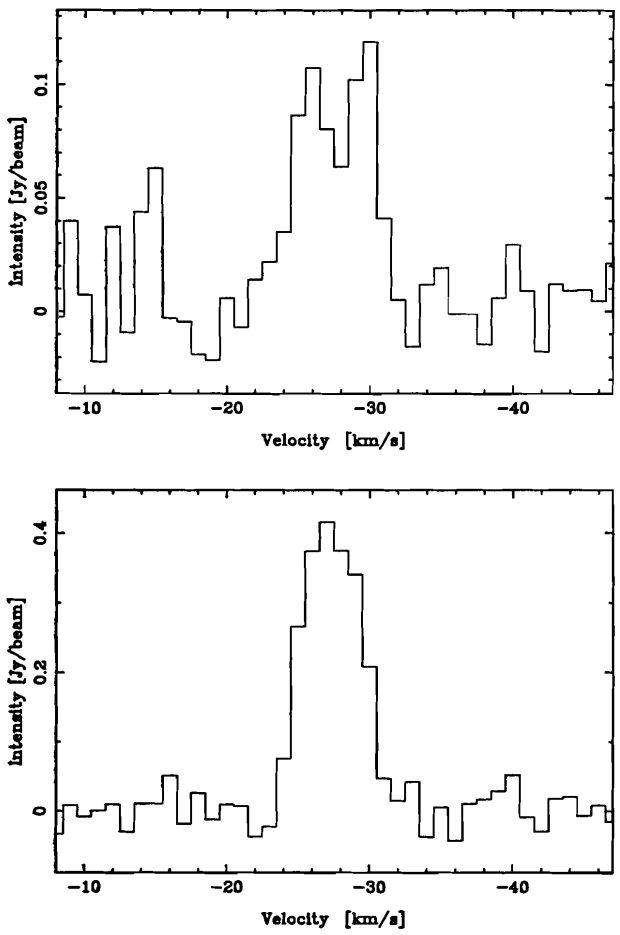

Fig. 3. CO(J=1 $\rightarrow$ 0 and J=2 $\rightarrow$ 1) spectra obtained towards the position of TT Cyg (upper and lower panel, respectively). The feature at ~–15 km s^{-1} in the J=1 $\rightarrow$ 0 spectrum is due to emission from the shell

emission is missed by the interferometer. However, there is a clear trend over the line. At the line centre the interferometer flux has its maximum relative to the single-dish flux (~90%). This points towards an emission that is not more widely distributed in the radial direction than what is seen in the interferometer maps close to the systemic velocity, i.e., all the CO emission comes from a narrow shell. If we assume that no flux is missed by the interferometer at the line centre (i.e., the interferometer fluxes are scaled by a factor 1/0.9 to correct for calibration differences between the interferometer and the single-dish data), we conclude that ~40% (~25%) of the extreme blue- (red-) shifted emission, where the emitting regions are two orders of magnitude larger than the FWHM of the synthesized beam, may be resolved out by the interferometer. The shortest projected baseline corresponds to an angular resolution of ~30″ and ~15″ in the J=1 $\rightarrow$ 0 and J=2 $\rightarrow$ 1 lines, respectively. In the J=1 $\rightarrow$ 0 line this is comparable to the sizes of the emitting regions at the extreme velocities, and so some of the missing flux may come from extended emission. It is possible that part of the effect at the extreme velocities is also due to the difficulties in CLEANing the dirty images in these velocity ranges where the emission is very extended. In conclusion, these results are consistent with the CO emission coming mainly from a geometrically thin shell consisting of a clumped medium.

The J=2 $\rightarrow$ 1 interferometer map does not cover the entire shell (in some velocity ranges it is missed altogether), and we can only make a crude comparison for the emission around the systemic velocity. Only about 45% of the single-dish flux is present in the interferometer data. This can be partly attributed to the limited coverage of the shell. About 20% of the emitting area is not covered, see Fig. 2, and hence in a large fraction of the shell at least 65% of the J=2 $\rightarrow$ 1 single-dish flux is present in the interferometer data. Considering the results for the J=1 $\rightarrow$ 0 data and the resolution obtained in the J=2 $\rightarrow$ 1 line for the shortest baseline, we would expect only little flux ($\lesssim$10%) to be missed at the systemic velocity in the J=2 $\rightarrow$ 1 data. Therefore, there is possibly a discrepancy in the absolute calibration of the interferometer and single-dish data.

4.2. The global shell geometry and structure

The impression obtained from Fig. 1 is that the emission arises in a very thin shell with a high degree of circular symmetry. This is emphasized in Fig. 4 where a circular ring, with a Gaussian intensity distribution in the radial direction, has been fitted to the J=1 $\rightarrow$ 0 data in the –27.5±2 km s^{-1} interval. The radius of the ring is 34.″7 and its full width at half maximum is 3.″2 (when deconvolved with a 2″ beam the shell width is 2.″5). However, the centre of the ring is offset 1.″8 [PA~-16°; in the

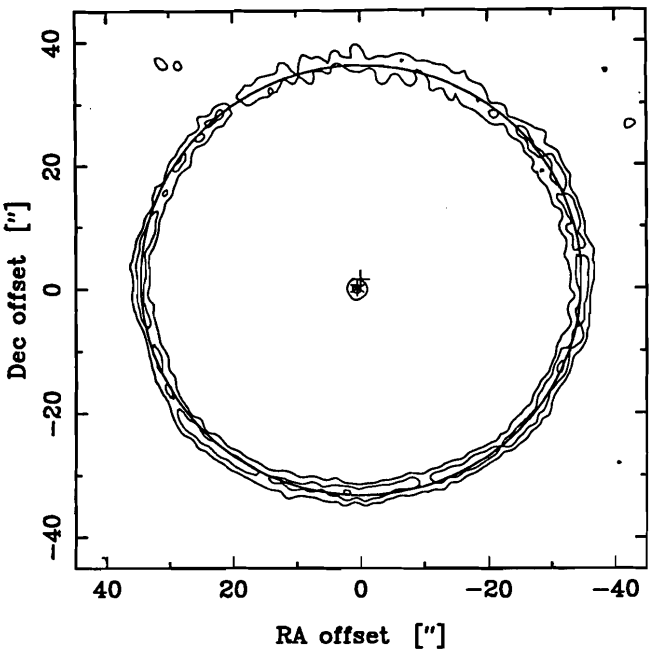

Fig. 4. A fit of a circular, Gaussian ring to the CO(J=1→0) data in the –27.5±2 km s^{-1} interval. The centre of the ring is marked with a +, and the position of the star (here given by the peak position of the central emission) with an *. The contours lie at 30, 60, and 90% of the maximum intensity

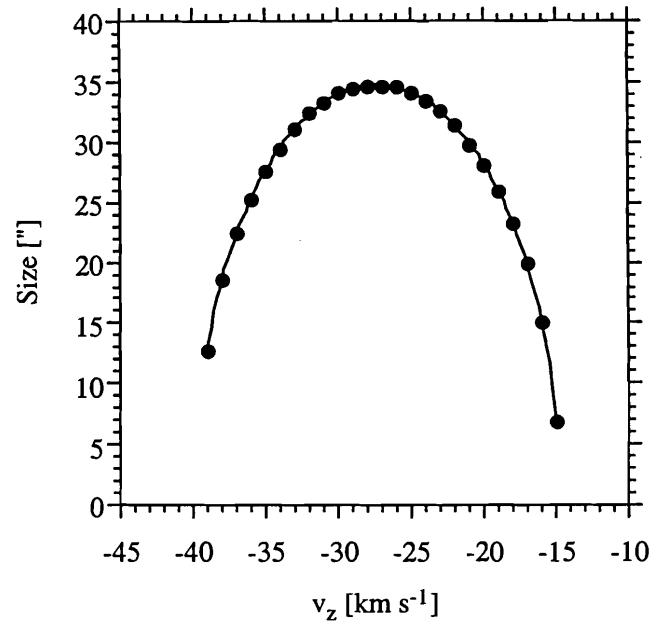

Fig. 5. The estimated shell sizes as a function of line-of-sight velocities for the CO(J=1→0) data, and the best fit of the relation $R_s\sqrt{1-[(v_z-v_*)/v_e]^2}$ to these data (see text for details). The 1σ errors of the size estimates lie in the range 0.″01 (at the systemic velocity) to 0.″08 (at the extreme velocities)

following the position angle (PA) is counted from the north to the east] with respect to the position of the star (here given by the peak position of the central emission). We will analyze this offset further in Sect. 4.4.

We have also fitted circular, Gaussian rings to all the J=1→0 brightness maps shown in Fig. 1, in order to study the 3D-geometry of the shell. There are only small deviations from circular symmetry in all velocity intervals. The results are shown in Fig. 5, where the ring radius is plotted versus the line-of-sight velocity. The best fit of the relation $R_s\sqrt{1-[(v_z-v_*)/v_e]^2}$ is also shown. The shell is expected to obey this relation if it is spherically symmetric and expands with the same velocity in all directions, in which case v_* is the systemic velocity and v_e is the gas expansion velocity. An excellent fit is obtained for R_s=34.″78±0.″03, v_*=–27.33±0.01 km s^{-1}, and v_e=12.58±0.01 km s^{-1} (the errors only indicate the goodness of the fit to the data points). This strongly suggests that the shell has a remarkable overall spherical symmetry. The linear average shell radius and width are ~2.7×10^{17} cm and ~1.9×10^{16} cm, respectively. The dynamical time scales, τ=r/v_e, for the shell radius and width are ~6800 yr and ~500 yr, respectively. We will adopt –27.3 km s^{-1} and 12.6 km s^{-1} as the systemic and expansion velocities of the shell, respectively (thus, the maps in Figs 2 and 4 are all centred within 0.2 km s^{-1} of the estimated systemic velocity). The systemic velocity estimated from the central emission agrees exactly with the result for the shell.

For a thin, approximately spherical shell that expands with a constant velocity a relatively accurate reconstruction of the 3D-geometry may be obtained. We have used the CO(J=1→0) data to produce Mollweide projections of the shell radius (here defined as the distance of the shell to its centre), the shell width, and the observed brightness, Fig. 6. The shell centre is obtained from the fit shown in Fig. 4. In the final stage the results are smoothed to a resolution of ~10° on the sphere. This is done to minimize effects due to the limited angular and spectral resolutions of the observations. The effect of the interferometer missing flux from extended emission is most severe in the regions where the gas moves directly towards (the extreme blue-shifted emission) and away (the extreme red-shifted emission) from us (see Sect. 4.1), and we have therefore blanked the results in two cones, with opening angles of 60°, directed towards and away from us. In principle, parts of the structure in Fig. 6 could be due to an expansion velocity that varies with direction, and hence causing an error in the deprojection. It is difficult to estimate whether or not this is the case. However, we find that e.g. the variations in the estimated shell radius over the sphere are very similar to those estimated from the data close to the systemic velocity (i.e., where projection effects play a very limited rôle, see Fig. 10). Thus, we believe that expansion velocity variations have a negligable effect on the results in Fig. 6.

The results presented in Fig. 6 emphasize the overall spherical symmetry. The shell radius is calculated as the intensity-weighted distance. All distances lie within ±3%, i.e., within ±1″, of the average distance 34.″8. There are no apparent trends, but there are regions where the shell is systematically curved inwards or outwards.

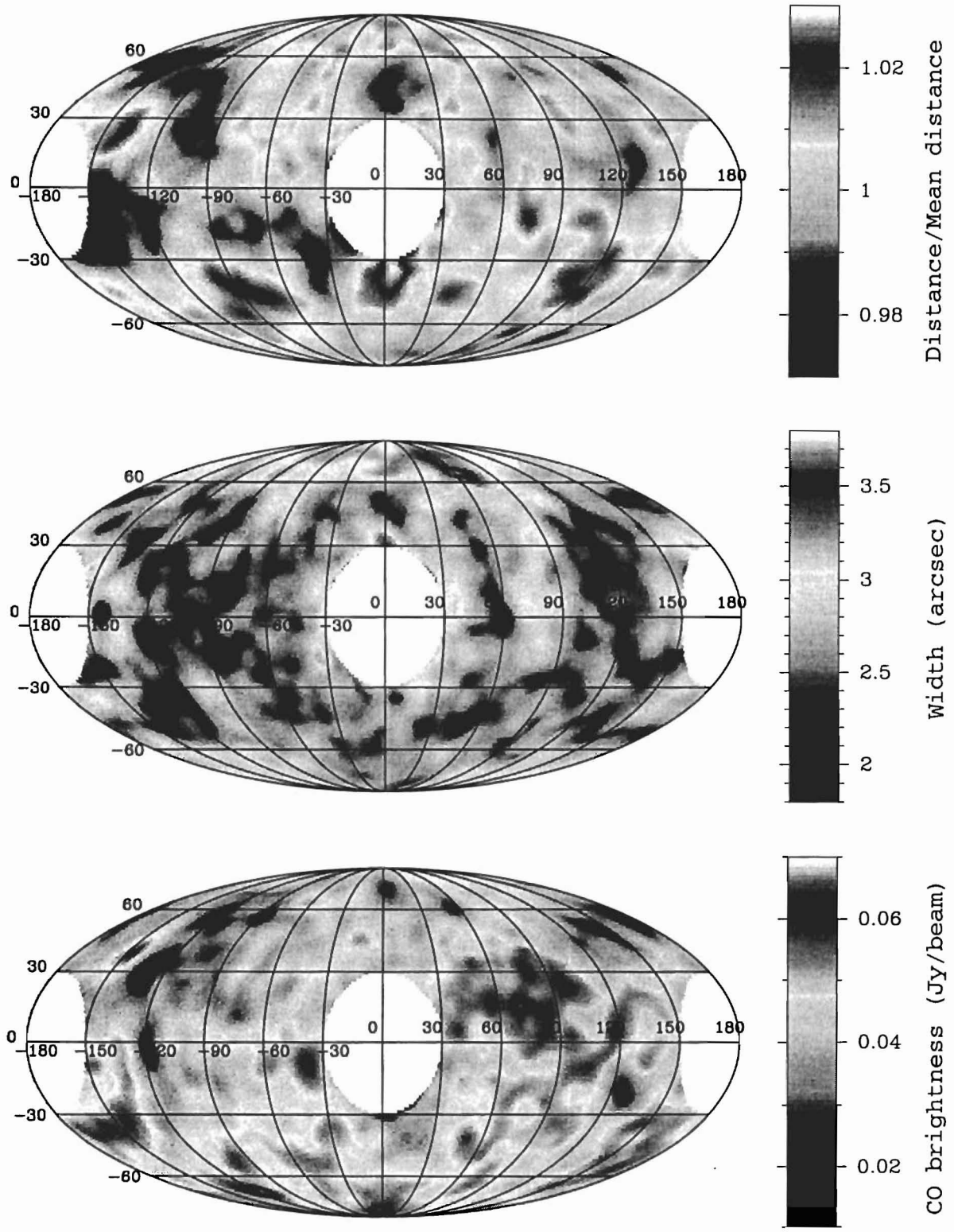

Fig. 6. Top: The distance of the shell to its centre, in units of the average distance, as estimated from the CO(J=1 → 0) data (upper). **Middle:** The width of the shell, in arc seconds, as estimated from the CO(J=1 → 0) data (middle). No correction for the beam smearing has been done. **Bottom:** The observed CO(J=1 → 0) brightness, in Jy beam^{-1}, of the shell (lower). The results of the deprojection are smoothed to a resolution of 10° on the sphere (see text for more details). The results in cones of opening angle 60° directed towards and away from us have been blanked

The width is obtained from the standard deviation of the distance estimate, but given in terms of a full width at half maximum of a Gaussian distribution. This should not be taken as the true shell width that would be obtained from a Gaussian fit in the radial direction, but the result reflects any trends there are. The broadening due to the ~2″ beam has not been removed. There is a clear large-scale trend in the sense that the shell is markedly thicker towards its northern pole.

The observed CO(J=1→0) brightness of the shell (note that this is not the surface brightness that would be seen from directions perpendicular to the shell surface) is patchy with a variation on a large angular scale by at least a factor of three between different regions. In particular, the lower hemisphere is markedly brighter than the upper one. Thus, the brightness decreases in this region where the shell broadens. It therefore seems that the variation in the total emission is more limited. We have used the Gaussian fits to the radial J=1→0 intensity distributions (in the $-27.5\pm2\,\mathrm{km\,s^{-1}}$ interval) presented below in Fig. 9, to show that the product of the intensity and width varies considerably less with position angle than the deconvolved width and somewhat less than the intensity, Fig. 7. Even though the width of the shell varies by about a factor of three and the brightness by about a factor of two, the variation in the total intensity is rather moderate (the standard deviation is 0.15 for the normalized product). This may suggest that the amount of material in the shell is rather evenly distributed on the larger scale (i.e., at least when averaged over solid angle intervals of about 0.2 steradians). Of course, one should caution here that there is not necessarily a one-to-one relationship between brightness and density distribution, e.g., due to saturation. On the other hand, there are several processes that tend to make the brightness distribution have more contrast than the density distribution, e.g., photodissociation and excitation.

We will finally analyze in yet another way the global distribution of the CO line-emitting material in the shell. Each map in Fig. 1, which covers emission from a $1\,\mathrm{km\,s^{-1}}$ interval, contains emission from $1/2v_e$~4% of the volume of the shell (for a spherical shell of radius R and width ΔR that expands with the velocity v_e the volume emitting radiation in the narrow velocity range Δv around the line-of-sight velocity v_z is given by $2\pi\Delta R R^2\Delta v/v_e$, i.e., independent of v_z, and the full velocity width of the emission is $2v_e$). Thus, we expect each map to contain the same amount of emission if the emitting material is uniformly distributed on the large scale and the emission is optically thin. Similarly, if the emission is optically thick but the medium consists of a large number of small clumps that are uniformly distributed (with only limited amounts of shadowing), each map will contain the same amount of emission. If the emission is optically thick and the medium is smoothly distributed we expect the emission to decrease towards the systemic velocity. In Fig. 8 we show the product of the shell brightness, the shell width, and the shell size for each map (obtained from the fits of Gaussian circles), i.e., a measure of the total emission from each map. Except for the two extreme velocity maps (where the effects of resolution on the interferometer fluxes are expected to be present) the product is essentially constant. This excludes a smooth, optically thick medium, and points to optically thin emission or, more likely considering the discussion in Sect. 4.1, a highly clumped medium that may be optically thick. Furthermore, averaged over the scales of the maps in Fig. 1 the CO gas appears to be evenly distributed over the shell. The constant product, which is lower by about 50% only at the two extreme velocities, also strengthens the above conclusion that resolution effects in the interferometer data are quite limited.

We will end this section by examining the CO brightness distribution across the shell, i.e., the radial CO bright-

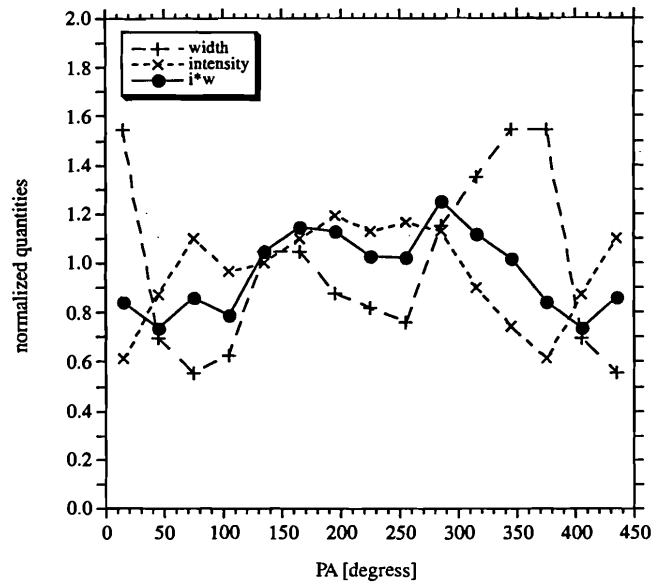

Fig. 7. The normalized (with the respective average values) intensities, deconvolved widths, and products of intensity and width obtained from the Gaussian fits to the CO(J=1→0) data presented in Fig. 9. Note that the data in the 0–90° interval are repeated at the end

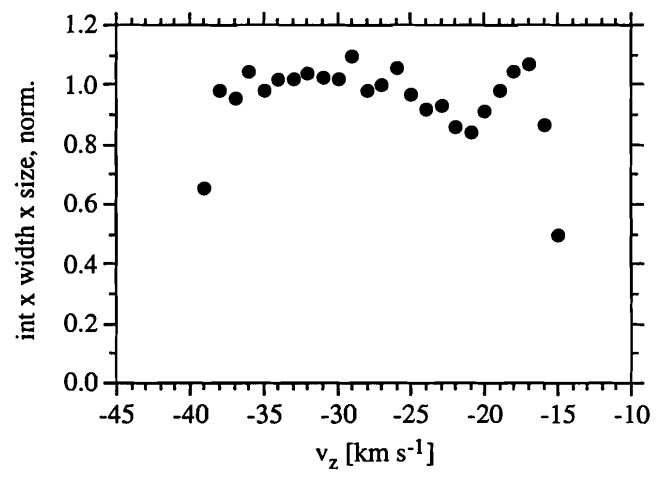

Fig. 8. The products of the intensities, widths, and sizes, obtained from the fits to the CO(J=1→0) shell emission, plotted against the line-of-sight velocity (the results are normalized to the value for the $-27\,\mathrm{km\,s^{-1}}$ map)

ness distribution. Once again, we use the J=1 → 0 data in the –27.5±2 km s^{-1} interval, for which we have estimated that very little, if any, of the flux is missed by the interferometer. The data are averaged over position angle intervals of 30° and then presented in 0.″5 bins in Fig. 9. Obviously, there is also an averaging along the line-of-sight. These radial brightness distributions are essentially perfectly fitted by Gaussians in all PA-intervals. That is, although the shell is resolved (marginally in some PA-intervals), we find no clear evidence for any structure in the radial brightness distribution, e.g., an edge brightening. The radial brightness distributions also show low-intensity large-scale undulations that must be attributed to the problem of CLEANing such a complicated image. However, this also puts limits on any low-intensity structure that can be identified. Thus, we cannot confirm the indications of weak J=1 → 0 emission on the inside of the shell that was reported by Olofsson et al. (1998) for a limited PA-interval. Here we conclude that any emission immediately inside or outside the shell is weaker than ~5% of the shell peak brightness when azimuthally averaged over the 0°–360° interval.

4.3. Shell radius, width and CO brightness variations

It has been shown in the preceding section that the shell has an almost perfect overall spherical symmetry, and that the CO(J=1 → 0) emission is relatively uniformly distributed over the shell when averaged over sufficiently large solid angles (about 0.2 steradians). We shall in this section analyze the radius, the width, and the CO brightness of the shell in more detail, although using data from only parts of the shell. The best estimates of the radius and width are obtained from the maps centred around the systemic velocity. It appears that very little of the total flux is missed by the interferometer at these velocities, see Sect. 4.1. We will use the results from the Gaussian fits to the radial J=1 → 0 brightness distributions presented in Fig. 9. We have done the same thing for the J=2 → 1 data in the –27.5±2 km s^{-1} interval and in the PA-intervals where reliable estimates can be obtained. We caution once again that the J=2 → 1 data may miss significant amounts of flux, something which may affect, in particular, the width estimates. The results are summarized in Fig. 10.

The radii estimated from the J=1 → 0 and J=2 → 1 data agree almost perfectly. There are clear smooth variations in the shell radius, but the difference between the maximum and minimum radius is only 1.″2. Likewise, the widths (deconvolved full width at half maximum) estimated from the J=1 → 0 and J=2 → 1 data agree reasonably well. There is a considerable variation in the shell width (in the J=1 → 0 data that cover the full PA-range), with a minimum of ~1.″3 at <PA>=75° and a maximum of ~3.″7 at <PA>=0°, i.e., the width varies between 1 and 3×10^{16} cm, and the corresponding time scale range is 250 to 750 yr provided that the gas expansion velocity can be used in estimating this. The width/radius ratio ranges from ~0.04 to 0.1. There is a trend that the shell distance to the centre is larger in those areas where the shell is geometrically thicker.

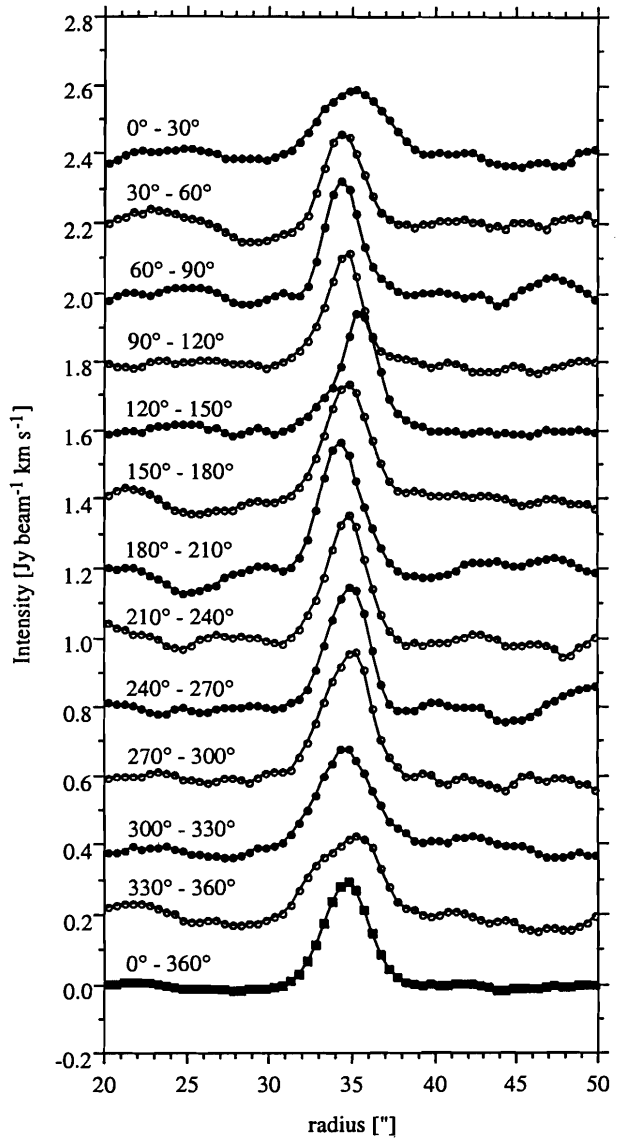

Fig. 9. The radial CO(J=1 → 0) brightness distributions, in 0.″5 bins, averaged over position angle intervals of 30° and integrated over the velocity interval –27.5±2 km s^{-1}, starting with the 0°–30° interval at the top to the 330°–360° interval (alternating filled and open circles, with the curves offset by 0.2 Jy beam^{-1} km s^{-1} with respect to each other). The lowest curve shows the result for the entire 0°–360° interval (filled squares). The radial distance is measured from the estimated shell centre

The detailed brightness distribution is most clearly seen in the maps obtained close to the extreme velocities, where the line-of-sight is almost in the radial direction through the shell. In order to avoid as much as possible resolution effects we have chosen to present the J=1 → 0 map centred at –38 km s^{-1}, Fig. 2. This map contains emission from ~4% of the shell volume (see above). Using the same line of arguments as that in Sect. 4.1 we estimate that it contains ~60% of the single-dish flux from this region. Thus, we can expect that there is only a limited enhancement of the small-scale structure in the interferometer data. The brightness distribution is very patchy, and

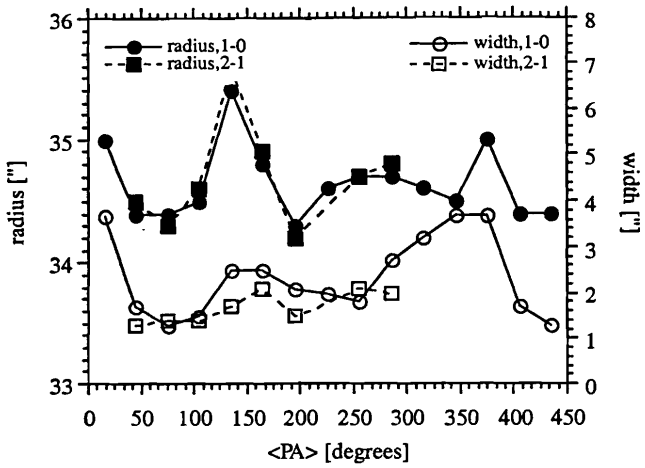

Fig. 10. The shell radius and width (deconvolved full width at half maximum), estimated from the CO(J=1→0 and J=2→1) data in the –27.5±2 km s^{-1} interval, are shown as a function of the position angle. Note that the J=1→0 data in the 0–90° interval are repeated at the end

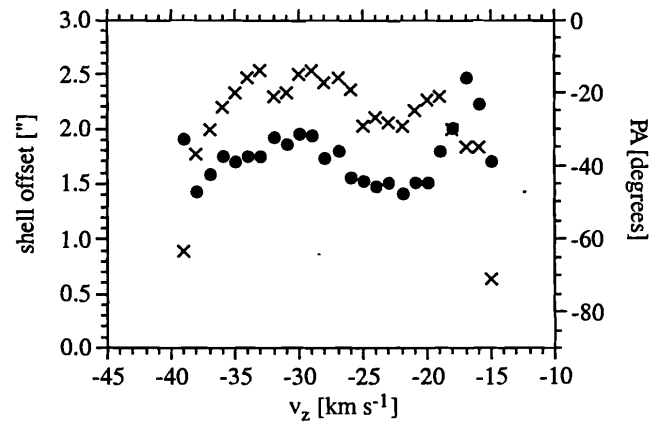

Fig. 11. The offsets to the position of the central emission of the centre of the rings, fitted to the CO(J=1→0) data shown in Fig. 1. The sizes of the offsets are denoted by filled circles, and the position angles by crosses

there are regions with only very weak emission. The size scale appears to be set largely by the resolution, suggesting that there is unresolved emission. We will discuss this suggested clumpy structure further in Sect. 4.5.

4.4. The shell centre

The centre of the Gaussian ring fitted to the J=1→0 data in the –27.5±2 km s^{-1} interval (Fig. 3) is offset 1.″8 (PA∼–16°) with respect to the peak position of the central J=1→0 emission. The latter agrees well with the Hipparcos position of the star. In Fig. 11 we show the results of fits of rings to all the J=1→0 brightness maps of Fig. 1. The result is a roughly constant offset by ∼1.″7 at a PA∼–20° in the velocity range –27.5±9.5 km s^{-1}. Outside this range the offsets and the position angles start to vary, but this is also the regions where the emission becomes very extended and the uncertainties in the fits increase significantly.

The essentially circular form of the brightness distributions, and the roughly constant offset as a function of the line-of-sight velocity (and hence the distance along the line-of-sight), suggest to us that the offset between the star and the shell centre is an effect of a relative motion between the two, rather than due to asymmetric expansion of the shell. Thus, the reason for the offset is probably not a consequence of the ejection nor of an interaction with an asymmetric or moving surrounding medium. We note that the average line-of-sight velocity of the interstellar molecular medium is ∼10 km s^{-1} in the direction of TT Cyg, i.e., very different from the velocity of TT Cyg). Thus, effects of interaction with the ISM cannot be entirely excluded, in particular since the shift is towards the north where the shell seems to be breaking up. On the other hand, one would have expected detectable departures from circular symmetry, since in this case the shell must expand 12.6 km s^{-1} × (2 × 1.″7/34.″8) ∼ 1.2 km s^{-1}, or by 10% of the full expansion velocity, faster towards the north. Also, a deformation of the shell should cause a trend in the offsets along the line-of-sight. Finally, TT Cyg has a proper motion of 6.3±1.0 mas yr^{-1} (PA∼–120°) as measured by Hipparcos. This means that the star and the shell have moved ∼40″ in the tangential direction since the ejection of the shell (assuming constant expansion velocity), and hence that any possible interaction between the shell and the surrounding medium is likely to be very weak. We have not detected any interstellar CO emission in the direction of TT Cyg. An upper limit on the density of the interstellar medium of ∼0.03 cm^{-3} is required to have a mean free path longer than 3×10^{17} cm (corresponds to ∼40″ at the distance of TT Cyg). Nevertheless, a reasonable explanation to the large scale variation of the shell width may be some kind of interaction with surrounding gas, albeit a fairly weak one.

If the offset is interpreted as due to relative motion between the shell and the star the tangential velocity difference between the star and the shell can be estimated to be 12.6 km s^{-1} × (1.″7/34.″7) ∼ 0.6 km s^{-1}. This result is independent of the distance, but assumes that the shell expansion velocity can be used to estimate the time scale (we find no difference in the systemic line-of-sight velocities of the centre and the shell emission, but the uncertainties of these estimates, in particular that of the centre emission, is estimated to be at least 0.5 km s^{-1}). Such a velocity difference could be due to the star being a member of a binary system. In all likelihood the mass of the companion is lower than that of TT Cyg (a less massive companion would be on the main sequence, while a more massive companion should have reached the white dwarf stage). Very crudely, assuming that TT Cyg and its companion both have a mass of ∼1 M$_\odot$, the observed velocity of TT Cyg suggests a wide binary with a semi-major axis of ∼1300 AU, or ∼3″ (the distance between the two stars decreases if the companion is less massive than TT Cyg). If the companion is still on the main sequence its luminosity would be comparable to,

or less than, that of the Sun, and a star with a solar luminosity would have a visual magnitude of ~13, which would be difficult to detect in the vicinity of the very bright carbon star (m_V~7.5^m). However, towards the blue the brightness contrast improves in favour of the warmer star. The companion should be found along a line with a PA~70°. The estimated orbital velocity is so low that any motion of TT Cyg during the shell ejection will have negligable effects on the shell structure. Likewise, the binary system is so wide that it should have no effect on the geometry of the mass loss.

4.5. The properties of the molecular medium

We will make a crude estimate of the molecular mass of the shell and its physical state, assuming uniform density and temperature in the shell. In this case the derived results depend to a large extent on the assumed CO abundance. The CO column density is partly constrained by the observed intensity, and hence gives the H_2 density, n_{H_2} (for a given shell width). Likewise, n_{H_2} and the gas kinetic temperature, T_k, are jointly constrained by the line intensity ratios, and hence this determines T_k. We have used the same radiative transfer model as referred to in Sect. 3, and adopt $f_{CO}=10^{-3}$ and a shell width of 2×10^{16} cm. The density and temperature are not well constrained by the observational data. We use our J=1→0 and J=2→1 spectra obtained towards the shell centre with the IRAM 30 m telescope (Olofsson et al. 1996), as well as a J=3→2 spectrum, obtained by us at the Caltech Submillimeter Observatory, with T_{mb}~0.25 K at the extreme velocity peaks. Acceptable fits to the observational data can be obtained for a range of values where the product $n_{H_2}\sqrt{T_k}$ is roughly constant. Low and high temperature solutions are excluded, but good fits are obtained in a region centered on n_{H_2}~250 cm^{-3} and T_k~100 K. This results in a shell mass of ~0.007 $M_\odot$. The density and the temperature estimates scale roughly as f_{CO}^{-1} and f_{CO}, respectively, and the shell mass roughly as $f_{CO}^{-1}D^2$ (D is the distance). The emission is optically thick; the tangential optical depths are about 1.5 and 2.5 in the J=1→0 and J=2→1 lines, respectively, a result inconsistent with the fact that the emission in each 1 km s^{-1} map is essentially the same, see Sect. 4.2. This suggests a clumpy medium. The kinetic temperature is very high at this distance from the star suggesting either a lower f_{CO} or an efficient heating mechanism. However, if the medium is clumped the data can be fit with considerably higher densities and consequently lower temperatures. In the homogeneous model the estimated CO and H_2 column densities are not enough to protect the CO molecules from photodissociation; the photodissociation time scale is ~10^3 yr using the results of van Dishoeck & Black (1988) for an average interstellar UV field [to reach a photodissociation time scale of ~10^4 yr requires a CO (H_2) column density of ~6×10^{16} cm^{-2} (~6×10^{19} cm^{-2}), and consequently a molecular shell mass of ~0.1 $M_\odot$]. This again suggests a clumped medium. A mass estimate for a clumped medium will depend on the clump sizes and their temperatures (Olofsson et al. 1996). At present there exists no acceptable model from which these quantities may be derived. Our estimate of 0.007 $M_\odot$ for the shell mass may be a severe underestimate due to the neglect of the clumpiness in the model.

However, we can use the data to make a schematic estimate of the clumpiness of the shell molecular gas. The essentially constant total emission from the 1 km s^{-1} maps and the morphology of the J=1→0 brightness distributions at the extreme velocities suggest that the gas density distribution must, to a large extent, be clumpy on a size-scale less than ~2″, see Sects 4.2, and 4.3. To this we can add the above results from the smooth shell model. The single-dish data further suggest that the emission is optically thick, since in the central velocity range the J=2→1 flux is about four times higher than the J=1→0 flux (see Table 1), i.e., what is expected from blackbody radiation in the Rayleigh-Jeans limit. It is difficult to estimate the individual clump brightnesses, but the data presented in Fig. 2 indicate an average peak clump brightness of ~0.05 Jy beam^{-1}. Assuming the clumps to have Gaussian brightness distributions with FWHM:a of 0.″5 and 2.″0, we estimate that each clump should produce a J=1→0 main beam brightness temperature of ~0.01 and ~0.02 K, respectively, in the IRAM 30 m telescope (the brightness temperatures are ~20 and ~2 K, respectively). We also estimate that each clump contributes this intensity over a velocity range less than 1 km s^{-1}, based on the facts that the full widths at half maximum of the extreme spectral features in the single-dish spectra are ~1 km s^{-1} (Olofsson et al. 1996), and that there is very little spatial overlap between the 1 km s^{-1} maps outside the systemic velocity. The total integrated J=1→0 intensity of the shell emission is ~80 K km s^{-1} in the IRAM 30 m telescope (in the main beam brightness scale), and therefore ~7300 and ~3800 clumps are required to produce this emission if the clump sizes are 0.″5 and 2.″0, respectively. In terms of number of clumps per 1 km s^{-1} interval this corresponds to ~290, and ~150 clumps. These estimates are lower limits since we assume no overlap in the calculation of the total emission. The volume filling factors are ~0.01 and ~0.4 for the 0.″5 and 2.″0 clumps, respectively. Thus, the appearance of the brightness maps should be very different in the two cases, and this can be used to put some further constraints on the clump properties.

We have calculated the observed brightness distributions from a number of randomly distributed "Gaussian" clumps (with an optical depth of one through the centre in order to allow for some shadowing) within a shell such that Gaussian rings fitted to these artificial brightness distributions give the same results as the fits to the observed data. We have done this comparison for the –27 and –38 km s^{-1} maps, and the results for clump sizes of 0.″5 and 2.″0 are shown in Fig. 12. The peak brightness temperatures (in the J=1→0 line) of the 0.″5 and 2.″0 clumps are ~12 and ~3 K, respectively. It is clear that the brightness distributions produced by a larger number of small clumps have a morphology that resembles that of the observed data best.

Using the 0.″5 clump model and the derived shell mass we can make some crude estimates. The clump mass is of the order 10^{-6} $M_\odot$, i.e., ~1 $M_\oplus$. The average H_2 density in a

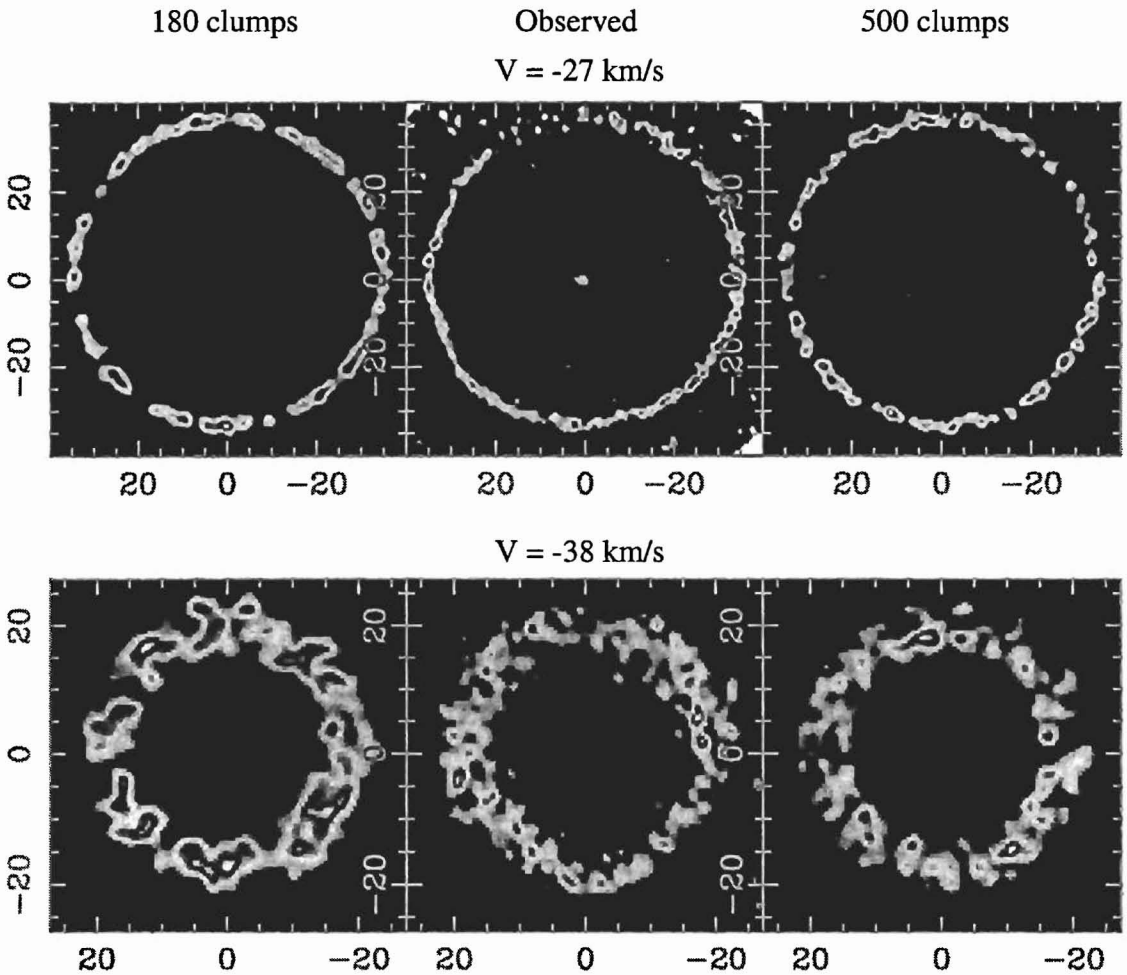

Fig. 12. Artificial brightness distributions compared with the observed –27 and –38 km s^{-1} CO(J=1 → 0) maps (middle panels). The artificial –27 km s^{-1} (–38 km s^{-1}) maps are produced by 180 clumps of size 2.″0 distributed in a 0.″8 (7.″3) broad ring (left panels), and 500 clumps of size 0.″5 distributed in a 3.″1 (7.″5) broad ring (right panels)

clump is $\sim 10^4$ cm^{-3} (this also results in a considerably lower kinetic temperature, $\lesssim$20 K, required to fit the observational data). The H_2 and CO column densities through a clump (diameter 8×10^{15} cm) are $\sim 6\times10^{19}$ and $\sim 6\times10^{16}$ cm^{-2}, respectively. Using these values and the results of the photodissociation model of van Dishoeck & Black (1988), we estimate a photodissociation time scale for CO of $\sim 10^4$ yr, i.e., as opposed to the case for the homogeneous shell this is enough to protect the molecules for a time scale comparable to the shell age, a conclusion reached also in Bergman et al. (1993) where the photodissociation was treated in some detail. This provides another strong argument for a highly clumped medium.

5. Possible scenarios for the shell formation

5.1. The case for a He-shell flash

Whatever the underlying cause of the shell is, it seems impossible to escape the conclusion that TT Cyg has gone through a period of considerable variations in its mass loss properties although the exact time scale is uncertain. Certainly, the expansion velocity of the gas must have been considerably higher in the past, and this normally means also a substantially higher mass loss rate. The ratio of the mechanical momentum rate of the shell gas and the radiation momentum rate is high, $[M_{\rm shell} v_{\rm e}^2/\Delta R]/[L/c] \sim 4$ (this could be even higher if the shell width, ΔR, is mainly due to broadening during the expansion, or considerably less if the gas is mainly swept-up during a longer time scale). Taken at face value it suggests a mass loss driven by radiation pressure on dust at the maximum possible rate, perhaps at a higher luminosity than the present one, or the presence of another mechanism. The corresponding ratio for the present mass loss epoch is 0.003.

TT Cyg is one out of five C stars with clearly detected detached CO shells: R Scl (radius $\sim$10″, a shell expansion velocity of 16 km s^{-1} results in a shell age of $\sim$1300 yr at a distance of 420 pc; Olofsson et al. 1996), U Cam (8″, 23 km s^{-1}, $\sim$800 yr at 500 pc; Lindqvist et al. 1999), U Ant (41″, 20 km s^{-1}, $\sim$2300 yr at 260 pc; Olofsson et al. 1996), S Sct (67″, 17 km s^{-1}, $\sim$8100 yr at 400 pc; Olofsson et al. 1996), and TT Cyg (35″, 13 km s^{-1}, $\sim$6800 yr at 510 pc).

The shell velocities are high when compared with the expansion velocities of normal envelopes of bright carbon stars (Olofsson et al. 1993). Within the considerable uncertainties the shell masses are all about 0.01 $M_\odot$ (Olofsson et al. 1996), except for the young shell around U Cam for which the shell mass is estimated to be $\sim$0.001 $M_\odot$ (Lindqvist et al. 1999). The three stars with the older CO shells have very low present mass loss rates, a few$\times 10^{-8}\,M_\odot\,yr^{-1}$, and low present wind velocities, $\sim$5 km s^{-1}. For U Cam a present mass loss rate of $\sim 2\times 10^{-7}\,M_\odot\,yr^{-1}$ and a present wind velocity of $\sim$12 km s^{-1} have been estimated (Lindqvist et al. 1999); for R Scl these quantities have not been possible to estimate due to the limited spatial resolution of the observations. The stars with detached CO shells belong to the sample of 68 visually bright C stars detected in circumstellar CO radio line emission by Olofsson et al. (1993), and they are all irregular or semiregular variables. The full sample of Olofsson et al. consists of $\sim$120 C stars, and it is expected to be reasonably complete in C stars out to a distance of $\sim$1 kpc. According to the calculation in Sect. 4.5 (see also Bergman et al. 1993) detached shells of this type are detectable in CO radio line emission for $\sim 10^4$ yr if the medium is clumped. The fraction of stars with detached CO shells suggests that the process responsible for the shell formation occurs on a time scale of $\sim 10^5$ yr. This is in fact the time scale between He-shell flashes for lower-mass C stars (Wagenhuber & Groenewegen 1998). Therefore, in our opinion the 'He-shell flash'-induced ejection of matter, suggested by Olofsson et al. (1990) and further elaborated by Vassiliadis & Wood (1993), Schröder et al. (1998, 1999), and Steffen & Schönberner (1999), remains the most reasonable explanation for the detached CO shells, and consequently also for the TT Cyg shell. We note here that Izumiura et al. (1997) used this scenario and the possible presence of two detached dust shells around U Ant to derive its present (high) core mass and its main sequence mass. Steffen et al. (1998) present an alternative origin for the detached shells. According to them, a narrow shell develops when the star is recovering to its normal luminosity, a few thousand years after the He-shell flash, and the wind goes from being shock-driven (low $\dot{M}$) to being dust-driven (high $\dot{M}$). However, the very low present mass loss rates of our stars suggest that they are not presently increasing their mass loss rates above the dust-driven wind limit. Although this mechanism may work we find this an unlikely explanation for the existence of the CO shells.

It is somewhat puzzling that the only C stars with detected CO shells are all members of the Olofsson et al. (1993) sample. Afterall, it represents only about 10% of all AGB-stars detected in circumstellar CO. This sample is clearly dominated by low mass loss rate objects (mainly irregulars and semiregulars), as opposed to most other surveys that have concentrated on higher mass loss rate objects (e.g., selected based on the IR-colours). It is conceivable that also the high mass loss rate objects have detached CO shells, but their contrast (in the CO radio line emission) against the normal envelope emission is much lower, and their on average larger distances make the spectral features of the shell emission (markedly double-peaked if spatially resolved) less conspicuous. Schröder et al. (1998, 1999) suggest that the shells are extra prominent in low mass objects, since these can drive (by radiation pressure on dust) substantial mass loss only during a He-shell flash. This result is, however, dependent on a prescription for how the mass loss rate depends on e.g. the stellar luminosity and, in particular, the effective temperature.

In principle, one would expect to see detached CO shells also around similar M stars. However, this is not the case as shown in a recent survey of irregularly and semi-regularly variable M stars by Kerschbaum & Olofsson (1999), where 66 low mass loss rate objects were detected in circumstellar CO. According to Little et al. (1987) these stars very rarely, if ever, show any evidence of technetium in their atmospheres, and it is therefore not clear whether they have gone through a He-shell flash. So far, only a tentative detection of a detached dust shell around the M-Mira R Hya exists (Hashimoto et al. 1998). We note that Wood & Zarro (1981) argue, for other reasons, that this star is going through a He-shell flash. In view of the results by Schröder et al. (1998, 1999) one may speculate that the absence of CO shells around M stars is related to lower luminosities and/or the different composition(s) of their dust grains. Finally, we note that Knapp et al (1998) suggest that the presence of multi-component CO radio line profiles towards a number of C and M stars may be related to episodic mass loss.

Even if a He-shell flash induced mass ejection has caused the formation of the shell around TT Cyg, it is not clear how the present day properties of the shell relate to the variations of the stellar properties during the mass ejection. We can imagine two (extreme) scenarios in connection with this: i) all the material in the shell was ejected at a very high rate during a short period and it has subsequently evolved during the expansion, or ii) the ejected material has interacted with a previous slow stellar wind leading to a narrow shell of mainly swept-up gas. Below we discuss the pros and cons of these two scenarios. In Sect. 6 we present various ways to reach a better understanding of the shell formation process.

5.2. *A brief high mass loss rate period*

This is an attractive scenario since it relates the present density distribution in the shell more directly to the mass ejection, but it is not without difficulties. The mass loss rate must have been of the order 0.007 $M_\odot$/500 yr $\sim 10^{-5}\,M_\odot\,yr^{-1}$, which is no problem in itself. However, the ejection must have been very isotropic in mass – within a factor of two the same amount of material appears to have been ejected in all directions (averaged over about 0.2 steradians) –, and also in velocity – the ejection velocity must have been isotropic to within $\pm 3\%$, i.e., v_e varies by less than ± 0.3 km s^{-1}. In particular, the latter is surprising considering the (presumed) complexities of the mass loss process and the inhomogeneous density structure of the shell gas. This points in the direction of a coordination of the ejection, i.e., something that can be provided by a He-shell flash. Furthermore, one would expect the shell to broaden during expansion due to thermal/turbulent motion. We can put a limit to

the present random motion using the line shapes and the overlaps of the brightness distributions in nearby velocity intervals. This suggests a random motion less than $\sim$1 km s^{-1}. If this applies also to earlier times we expect a broadening of the shell by $\sim$3″, i.e., comparable to the shell width. Consequently, the ejection time scale may have been very short, perhaps substantially shorter than the time scale corresponding to the present shell width, $\sim$500 yr. During such a short period the mass loss rate must have been very high, perhaps even higher than what can be driven by radiation pressure on dust. Finally, it is most likely that the star was losing mass at some rate and probably at a lower velocity before the mass ejection, and some interaction with the previous wind could therefore be expected. We also note here the considerable variations in shell width, and in particular the broadening towards the northern pole, that may indicate the presence of an interaction at some level.

5.3. *Interacting winds and swept-up gas*

This scenario is reasonable, but it makes it far more difficult to relate the present properties of the shell to the mass ejection mechanism. There are obvious problems also with this scenario. The surrounding medium must be extremely homogeneous, since an interaction tends to enhance any asymmetries there are. Most likely such a medium consists of a previous slow stellar wind, rather than an interstellar medium (since the tangential proper motion of the star and the shell by $\sim$40″ since ejection has not led to any appreciable effects, see Sect. 4.4). In this scenario the mass estimate could be a severe underestimate unless substantial amounts of CO were still present in the slow wind and survived the shock (which may be possible considering the expected low shock velocity) or were produced in the swept-up post-shock gas. A lower limit to the slow wind average mass loss rate is roughly given by 0.007 M$_\odot$ / 7000 yr $\sim$ 10^{-6} M$_\odot$ yr^{-1}, a not impossible value for this type of C star although it is almost an order of magnitude higher than the median mass loss rate found by Olofsson et al. (1993) for their sample of bright carbon stars. The CO photodissociation radius of a 10^{-6} M$_\odot$ yr^{-1} wind is $\sim 10^{17}$ cm or $\sim$10″ (Mamon et al. 1988), i.e, very little CO would remain in the swept-up gas if it is relatively homogeneous. However, if the shell mass is severely underestimated, a considerably higher mass loss rate will result and this will impose a problem, since there is no evidence for any material outside the shell, the CO brightness contrast is at least a factor of ten.

The conditions in the circumstellar environment of an AGB-star are such that an interaction between two stellar winds is not an unreasonable event. A 10^{-6} M$_\odot$ yr^{-1} wind will have an H_2 density of $\sim 150 \times r_{17}^{-2}$ cm^{-3} if the expansion velocity is 10 km s^{-1} (r_{17} is the radius measured in units of 10^{17} cm). The mean time between collisions when such a wind interacts with a higher-velocity wind is $\sim 1 \times r_{17}^2 / v_{10}$ yr (v_{10} is the relative wind velocity in units of 10 km s^{-1}). Thus, for v_{10}=1 we get a collision time of $\sim$10 yr at the present location of the shell, i.e. considerably shorter than the expansion time scale. We can make some quantitative estimates using the formulae derived by Kwok et al. (1978) for a fully momentum coupled wind interaction with a strongly radiative shock. In steady state the shell velocity is given by

$$v_s = \frac{v_1 + (\dot{M}_2 v_1 / \dot{M}_1 v_2)^{1/2} v_2}{1 + (\dot{M}_2 v_1 / \dot{M}_1 v_2)^{1/2}}, \quad (1)$$

the shell mass by

$$M_s = \left[\dot{M}_1 \left(\frac{v_s}{v_1} - 1 \right) + \dot{M}_2 \left(1 - \frac{v_s}{v_2} \right) \right] t, \quad (2)$$

and the relative shell width by

$$\frac{\Delta R_s}{R_s} = \frac{kT_s}{\mu m_H} \frac{v_2}{v_s (v_2 - v_s)^2} \frac{M_s}{\dot{M}_2 t}, \quad (3)$$

where the subscripts 1 and 2 refer to the slow and the fast wind, respectively, and T_s is the kinetic temperature of the shell gas. As an example we choose $\dot{M}_1$=$\dot{M}_2$=10^{-6} M$_\odot$ yr^{-1}, v_1=10 km s^{-1}, v_2=20 km s^{-1}, T_s=100 K (see Sect. 4.5), and t=7000 yr, and obtain $v_s \sim 14$ km s^{-1}, $M_s \sim 0.005$ M$_\odot$, and $\Delta R_s / R_s \sim 0.01$, i.e., results comparable to those estimated for the TT Cyg shell except for the shell width, which is a factor of 4–10 smaller than the width of the CO emission. The density compression by a factor of 10–15 requires effective cooling of the post-shock gas. However, a simple calculation for the relevant conditions in the shell suggests that this cannot be provided by the gas. Dust cooling could be more effective if the temperature is high enough. We estimate that in the present shell the dust cooling time scale would be of the order 10^3 yr, which is marginally sufficient. The time scale for formation of CO in the swept-up gas is determined by the time scale for C to collide with O (or compounds thereof) and this is lower, by at least a factor of 10^3, than the collisional time scale. Considering the estimated density and temperature in the shell, this puts some severe doubts on the efficiency of CO production in the post-shock gas. Thus, the case for an interacting wind scenario is not fully convincing, but the time scales will decrease if the medium is highly clumped.

6. Conclusions and future work

We have made high spatial resolution and sensitivity CO(J=1 $\rightarrow$ 0 and 2 $\rightarrow$ 1) observations of the semiregular carbon star TT Cyg with the IRAM Plateau de Bure interferometer. They show that this star is surrounded by a large, geometrically thin shell of gas that expands with a velocity of $\sim$12.6 km s^{-1}. The age of the shell is estimated to be $\sim$7000 yr. It has an almost perfect overall spherical symmetry, e.g., its radius varies by less than $\pm$3% over the sphere. The width varies by a factor of three, but the emitting gas is rather evenly distributed when averaged over a solid angle of about 0.2 steradians. Assuming a homogeneous medium and f_{CO}=10^{-3}, we estimate a molecular hydrogen density of $\sim$250 cm^{-3}, a gas kinetic temperature of $\sim$100 K, and a mass of $\sim$0.007 M$_\odot$ for the

shell (adopting the Hipparcos distance of 510 pc). These estimates are rather uncertain since neither the density nor the temperature are well constrained by the observational data, and in addition there is good evidence for a highly clumped medium. There is no evidence for matter immediately inside or outside the shell. The brightness there is $\lesssim$5% of the shell peak brightness when averaged azimuthally. We find no evidence for any particular structure (i.e., deviations from a Gaussian distribution) in the radial direction of the shell brightness distribution. The shell centre is clearly displaced by $\sim$1.″7 (position angle $\sim$–20°) with respect to the star. We tentatively interpret this in terms of TT Cyg being a member of a binary system. We put forward several arguments for a shell medium that consists almost entirely of a large number of small ($\lesssim$1″) clumps: e.g., the patchy brightness distributions, the interferometer flux being close to the single-dish flux even in areas of very extended emission, the constant total emission as a function of line-of-sight velocity, and the protection of the CO molecules against photodissociation. In this case the density required to fit the observational data is much higher, $\sim 10^4\,\mathrm{cm}^{-3}$, and the kinetic temperature is considerably lower, $\lesssim$20 K.

TT Cyg is presently losing mass at a quite modest rate, $\sim 3\times10^{-8}\,\mathrm{M}_\odot\,\mathrm{yr}^{-1}$, and with a low expansion velocity, $\sim$3.8 km s^{-1}. Both values are low even when compared with the average values obtained for a sample of visually bright carbon stars, $\sim 1.5\times10^{-7}\,\mathrm{M}_\odot\,\mathrm{yr}^{-1}$ and $\sim$12.5 km s^{-1} The systemic velocities estimated from the centre and the shell emissions agree perfectly, and the final value is estimated to be very accurate, –27.3±0.1 km s^{-1} in the LSR system.

We argue that TT Cyg has gone through a phase of increased, coordinated mass ejection, that may be related to a recent He-shell flash. At this point, we do not know how the effects of this internal thermo-nuclear runaway is transferred to the mass ejection mechanism. It seems very likely that the star had a low-velocity wind with a moderate mass loss rate before the ejection. One would therefore expect some effects of interacting winds. Primarily, this may affect the morphology of the shell, as well as provide swept-up gas. To what extent these effects are present is still uncertain, and consequently also the details of the mass ejection.

It is clear that more work is required before the shell formation process is identified and understood in detail. The proposed scenarios (a brief high mass loss rate epoch and interacting winds with swept-up gas, in both cases possibly connected with a He-shell flash) can be tested in various ways. One possibility is to observe in detail detached CO shell sources with different shell ages. Statistically, the younger shells should contain less mass, and perhaps also have considerably larger widths if interacting winds play a rôle. The first interferometer results on the very young ($<10^3$ yr) shell around U Cam indicate that the linear width of the shell is very similar to that of the TT Cyg shell, but the shell expansion velocity is higher by about a factor of two, the mass is lower by almost a factor of ten, and the kinetic temperature is lower by a factor of two (Lindqvist et al. 1999). Taken at face values, and provided that the mass ejections of U Cam and TT Cyg were very similar, this would support an interacting wind scenario, but we caution here that these results are obtained assuming a homogeneous medium. One cannot exclude the possibility that the CO emission does not trace the density distribution, e.g., due to photodissociation or lack of excitation. Unfortunately, other molecular radio line emissions have been possible to detect only towards the youngest CO shells, U Cam (Bujarrabal & Cernicharo 1994; Lindqvist et al. 1996) and R Scl (Olofsson et al. 1996). Therefore, the development of alternative observational methods are important. An obvious possibility is to observe the dust emission with high spatial resolution. The relation between the dust and the gas is bound to be different in the two scenarios. Unfortunately, the angular resolutions of the IRAS and ISO observations have not been high enough for exploring the detailed structure of the CO shells. The detected dust shells, in which no CO emission has been found (Olofsson et al. 1993), seem to be much broader than the CO shells (Waters et al. 1994; Izumiura et al. 1996, 1997). Thus, the connection between these dust shells and the CO shells is not clear. We note that in the hydrodynamical simulations of Steffen et al. (1998) geometrically thick, detached dust shells are produced as a consequence of the long period of low mass loss rate following a He-shell flash. The first results using stellar light scattered (by atoms and/or dust) in the shell of U Ant suggest that at least the outer edge of the CO emission also defines a sharp decrease in the density distribution (González Delgado et al., in prep.).

It is also important to numerically simulate, including hydrodynamical effects and using a two-fluid medium (dust and gas), the evolution of expanding thin shells and interacting winds [see e.g., Mastrodemos et al. (1996), Steffen et al. (1998)]. Recently, Steffen & Schönberner (1999) have simulated the result of a He-shell flash induced mass ejection and subsequent wind interaction and obtain results that are very similar to those observed for the CO shell of TT Cyg. Considering the clumpy structure of the shell gas, the evolution of primordial structures and the development of new ones due to instabilities are interesting. Myasnikov et al. (in preparation) have shown that clumpy structures, of the type found in the TT Cyg shell, may be ascribed to the development of Rayleigh-Taylor instabilities in the interaction zone (comparable in size with the width of the TT Cyg shell) between a massive stellar wind and a previous slower and less massive one. If, on the other hand, the winds are clumpy already from the start, the interaction of the winds becomes a more complicated phenomenon to study. Furthermore, it is possible that the CO shells are related to the multiple spherical shells and halos seen around many planetary nebulae (Frank et al. 1994; Stanghellini & Pasquali 1995). Finally, the shell clumps may appear in compressed form in planetary nebulae. A beautiful illustration of this is provided by the cometary knots in the Helix nebula (O'Dell & Handron 1996). O'Dell & Handron estimate that there are about 3500 'detectable' cometary knots in the Helix nebula. Meaburn et al. (1998) found that the morphological properties of the knots are remarkably similar. Extinction and CO radio line emission both give knot masses and densi-

ties of $\lesssim 10^{-5}$ $M_\odot$ and $\sim 10^5$–10^6 cm^{-3}, respectively (Huggins et al. 1992; Meaburn et al. 1998). The diameters of the largest knots are $\sim 3\times 10^{15}$ cm, and the CO line widths are narrow, 1–2 $km\,s^{-1}$. One may conclude that the knot properties are relatively similar to those of our clumps, except for their higher densities and masses. On the other hand, we do not believe that the TT Cyg shell is related to the shell structures seen in the HST images of CRL2688 (Sahai et al. 1998). These correspond to a much shorter time scale, and may possibly be related to mass loss variations during the (long) pulsational cycles of the central star at the tip of the AGB and subsequent interactions.

Acknowledgements. We are dedicating this paper, which is based on data obtained with the IRAM interferometer on Plateau de Bure, to the victims, and their families, of the tragic accident on July 1st, 1999, of the téléphérique that gave access to the Plateau de Bure observatory.

We are very grateful to F. Schöier for performing the radiative transfer analysis of the centre and the shell emission. We are also grateful to the referee, Dr. N. Trams, whose constructive comments lead to a better presentation of our results. Financial support from the Swedish Natural Science Research Council (NFR) is acknowledged. JHB acknowledges support from the U.S. National Science Foundation through grant AST-9618523.

References

Adler D.S., Lo K.Y., Wright M.C.H., et al. 1992, ApJ 392, 497
Bergman P., Carlström U., Olofsson H. 1993, A&A 268, 685
Blöcker T. 1995, A&A 297, 727
Bujarrabal V., Cernicharo J. 1994, A&A 288, 551
Forestini M., Charbonnel C. 1997, A&AS 123, 241
Frank A., van der Veen W.E.C.J., Balick B. 1994, A&A 282, 554
Groenewegen M.A.T., de Jong T. 1994, A&A 282, 115
Gueth F., Guilloteau S., Viallefond F. 1995, In: Green D.A., Steffen W. (eds) Proc. of XXVIIth YERAC 95. Cambridge Univ. Press
Guilloteau S., Delannoy J., Downes D., et al. 1992, A&A 262, 624
Habing H.J. 1996, A&AR 7, 97
Hashimoto O., Izumiura H., Kester D.J.M., Bontekoe Tj.R. 1998, A&A 329, 213
Huggins P.J., Bachiller R., Cox P., Forveille T. 1992, A&A 401, L43
Izumiura H., Hashimoto O., Kawara K., Yamamura I., Waters L.B.F.M. 1996, A&A 315, L221
Izumiura H., Waters L.B.F.M., de Jong T., et al. 1997, A&A 323, 449
Kerschbaum F., Olofsson H. 1999, A&AS 138, 299
Knapp G.R., Young K., Lee E., Jorissen A. 1998, ApJS 117, 209
Kwok S., Purton C.R., Fitzgerald P.M. 1978, ApJ 219, L125
Lindqvist M., Lucas R., Olofsson H., et al. 1996, A&A 305, L57
Lindqvist M., Olofsson H., Lucas R. et al. 1999, A&A in press
Little S.J., Little-Marenin I.R., Hagen Bauer W. 1987, AJ 94, 981
Mamon G.A., Glassgold A.E., Huggins P.J. 1988, ApJ 328, 797
Mastrodemos N., Morris M., Castor J. 1996, ApJ 458, 851
Meaburn J., Clayton C.A., Bryce M., et al. 1998, MNRAS 294, 201
O'Dell C.R., Handron K.D. 1996, AJ 111, 1630
Olofsson H. 1996, Ap&SS 245, 169
Olofsson H., Carlström U., Eriksson K., Gustafsson B., Willson L.A. 1990, A&A 230, L13
Olofsson H., Eriksson K., Gustafsson B., Carlström U. 1993, ApJS 87, 267
Olofsson H., Bergman P., Eriksson K., Gustafsson B. 1996, A&A 311, 587
Olofsson H., Bergman P., Lucas R., et al. 1998, A&A 330, L1
Sahai R., Trauger J.T., Watson A.M., et al. 1998, ApJ 493, 301
Schröder K.-P., Winters J.M., Arndt T.U., Sedlmayr E. 1998, A&A 335, L9
Schröder K.-P., Winters J.M., Sedlmayr E. 1999, A&A 349, 898
Stanghellini L., Pasquali A. 1995, A&A 452, 286
Steffen M., Schönberner D. 1999, A&A, in press
Steffen M., Szczerba R., Schönberner D. 1998, A&A 337, 149
van Dishoeck E.F., Black J.H. 1988, ApJ 334, 771
Vassiliadis E., Wood P.R. 1993, ApJ 413, 641
Wagenhuber J., Groenewegen M.A.T 1998, A&A 340, 183
Waters L.B.F.M., Loup C., Kester D.J.M., Bontekoe Tj. R., de Jong T. 1994, A&A 281, L1
Willems F.J., de Jong T. 1988, A&A 196, 173
Wood P.R., Zarro D.M. 1981, ApJ 247, 247
Zijlstra A.A., Loup C., Waters L.B.F.M., de Jong T. 1992, A&A 265, L5